Geosci. Model Dev. Discuss., 7, 2705–2743, 2014
www.geosci-model-dev-discuss.net/7/2705/2014/
doi:10.5194/gmdd-7-2705-2014

Geoscientific Model Development Discussions
Open Access

MM5 v3.6.1 and WRF v3.2.1 model comparison of standard and surface energy variables in the development of the planetary boundary layer

C.-S. M. Wilmot, B. Rappenglück, and X. Li

Department of Earth and Atmospheric Sciences, University of Houston, Houston, Texas, USA

Received: 19 March 2014 – Accepted: 14 April 2014 – Published: 29 April 2014

Correspondence to: B. Rappenglück (brappenglueck@uh.edu)

Published by Copernicus Publications on behalf of the European Geosciences Union.

Abstract

Air quality forecasting requires atmospheric weather models to generate accurate meteorological conditions, one of which is the development of the planetary boundary layer (PBL). An important contributor to the development of the PBL is the land-air exchange captured in the energy budget as well as turbulence parameters. Standard and surface energy variables were modeled using the fifth-generation Penn State/National Center for Atmospheric Research mesoscale model (MM5), version 3.6.1, and the Weather Research and Forecasting (WRF) model, version 3.2.1, and compared to measurements for a southeastern Texas coastal region. The study period was 28 August–1 September 2006. It also included a frontal passage.

The results of the study are ambiguous. Although WRF does not perform as well as MM5 in predicting PBL heights, it better simulates most of the general and energy budget variables. Both models overestimate incoming solar radiation, which implies a surplus of energy that could be redistributed in either the partitioning of the surface energy variables or in some other aspect of the meteorological modeling not examined here. The MM5 model consistently had much drier conditions than the WRF model, which could lead to more energy available to other parts of the meteorological system. On the clearest day of the study period MM5 had increased latent heat flux, which could lead to higher evaporation rates and lower moisture in the model. However, this latent heat disparity between the two models is not visible during any other part of the study. The observed frontal passage affected the performance of most of the variables, including the radiation, flux, and turbulence variables, at times creating dramatic differences in the r^2 values.

1 Introduction

Due to a combination of complex chemical and meteorological interactions, Houston suffers from air pollution problems. Metropolitan traffic and a bustling refinery industry

GMDD
7, 2705–2743, 2014

generate primary pollutants as well as precursors for secondary pollutants such as ozone. Despite the simple topography of the area, Houston's proximity to the Gulf of Mexico leads to a complex meteorological system that is influenced by both synoptic-scale and local land–sea breeze circulations. Various studies examining the interaction between these forcings have often noted that some of the most severe ozone exceedance days have occurred during stagnant periods when local and synoptic forces have clashed (Banta et al., 2005; Rappenglück et al., 2008; Langford et al., 2010; Tucker et al., 2010; Ngan and Byun, 2011).

In order to alert people to potentially health-threatening pollution levels, numerical weather prediction (NWP) models coupled to chemical models are used to predict the weather and its subsequent effect on atmospheric chemistry for the area. Two such models are the fifth-generation Penn State/National Center for Atmospheric Research mesoscale model (MM5; Grell et al., 1994) and the Weather Research and Forecasting (WRF) model (Skamarock et al., 2008). The MM5 model has been used extensively to simulate meteorological inputs for use in air quality models such as the Community Multiscale Air Quality (CMAQ; Byun and Schere, 2006) model.

Some studies, such as that done by Mao et al. (2006), have examined MM5 in the capacity of a coupled model, endeavoring to understand how changing the meteorological forcings affects the atmospheric chemistry output. Similarly, Ngan et al. (2012) looked at MM5 performance in connection with the CMAQ model ozone predictions. Other studies, such as was done by Zhong et al. (2007), have instead looked directly at MM5 output in order to better understand the meteorological parameterizations most appropriate for the local area.

Although MM5 is still being used for research purposes, the next-generation WRF model is now in general use. Developers of MM5 physics have imported or developed improved physics schemes for WRF, such as discussed in Gilliam and Pleim (2010), who found that the errors in all variables studied across the domain were higher in MM5 than in either WRF run with a similar configuration or the WRF run with a more common configuration. Their final conclusion was that the WRF model was now at a superior

GMDD
7, 2705–2743, 2014

level to MM5 and should therefore be used more extensively, especially to drive air quality models. Hanna et al. (2010) tested the Nonhydrostatic Mesoscale Model core for WRF (WRF-NMM) against MM5 for boundary layer meteorological variables across the Great Plains, and Steeneveld et al. (2010) used intercomparisons between MM5 and WRF to examine longwave radiation in the Netherlands. Both of these studies came to the conclusion that in general, WRF outperformed MM5.

The common parameters examined in all of these previous studies are the planetary boundary layer (PBL) schemes and land surface models (LSMs), because in spite of improvements in predictions of standard atmospheric variables such as surface temperature and wind fields, characteristics of the PBL, especially PBL height, continue to elude modelers. For example, when Borge et al. (2008) did a comprehensive analysis of WRF physics configurations over the Iberian Peninsula, PBL height estimates for two observation sites were poor at night and during the winter, which are classically periods of stable boundary layer development. Other studies have found similar performance with PBL height (Wilczak et al., 2009; Hanna et al., 2010; Hu et al., 2010).

Although many of these studies examine the sensitivity of WRF to PBL scheme and LSMs, not as much attention has been given to evaluating the effects of the energy balance variables generated by these various schemes. The complex interaction between latent and sensible heat, radiation and ground flux all affect the performance of meteorological variables, which in turn affect boundary layer properties such as PBL height. Analyzing the performance of these variables within a model should give further insight into the mechanisms that affect boundary layer properties, but these energy balance variables are not as commonly evaluated in the model because of a lack of observations.

Variations of the PBL height play an important role in air quality. Studies performed during the first and second Texas Air Quality Study (TexAQS-2000, TexAQS-II) have noted an increase in ozone after a frontal passage in the Houston area (Wilczak et al., 2009; Rappenglück et al., 2010; Tucker et al., 2010). This study is conducted to determine how well the MM5 and WRF models simulate PBL height, variables affecting

GMDD
7, 2705–2743, 2014

its development, and standard atmospheric variables for a frontal passage during TexAQS-II.

2 Observational data, models, and statistical analysis

2.1 Location

The focus of this study is the University of Houston Coastal Center (UH-CC), which is located near the Gulf of Mexico coast (29°23′16.67″ N, 95°02′29.09″ W) and is surrounded by approximately 200 acres of prairie grass (Fig. 1). This location was selected both because it is the location of previous field studies (Clements et al., 2007; Zhong et al., 2007) and is clear of surrounding structures that would interfere with the natural meteorological processes. Its micrometeorological setup is comprehensively described in Clements et al. (2007). Most of the modeling and observation data was extracted from this location with the exception of the radiosondes, which were launched from the UH main campus (Rappenglück et al., 2008), and wind fields for the inner WRF domain, which were provided by the Texas Commission on Environmental Quality (TCEQ) Continuous Ambient Monitoring Stations (CAMS) in the surrounding area.

2.2 Observational data

2.2.1 Measurement tower instrumentation

During the study period 28–31 August 2006, both standard and energy budget surface variables were being measured (Table 2). Instrumentation included an R.M. Young 5103 anemometer to capture 10-mean wind speeds (WDIR10) and directions (WSPD10), a CST CS-500 temperature probe for 2 m temperature (TEMP2), and a Kipp & Zonen CNR1 four-component net radiometer to capture incoming shortwave (SWDOWN), incoming longwave (LWDOWN), outgoing shortwave (SWUP), and

GMDD
7, 2705–2743, 2014

outgoing longwave radiation. Sensible heat (SHFLUX) and latent heat (LHFLUX) fluxes were measured using REBS soil heat flux plates.

Measurements were taken at a frequency of 1 Hz and averaged to 1 min (TEMP2, Q2, WSPD10, WDIR10) and 10 min (SWDOWN, LWDOWN, SWUP, SHFLUX, LHFLUX, GRNDFLUX). All measurements were then averaged to one hour to compare to the hourly model data.

2.2.2 Radiosonde data

Radiosondes were not directly measured at the UH-CC during this study period, but were regularly launched from the UH main campus approximately 40 km away. RS-92 GPS sondes were used (Rappenglück et al., 2008). The difference in potential temperature vertical lines between the grid point representing the UH-CC and the UH was zero, which gave confidence that PBL heights measured at UH provide a reasonable approximation for model comparison at the UH-CC. Launches were performed at 06:00 CST and 18:00 CST for the first two days of the study period, and more were launched during the final two days of the study (Table 2). PBL heights were determined to be the height at which potential temperature begins to increase (Rappenglück et al., 2008). The first radiosonde launch was discarded for purposes of statistical analysis because it corresponded to the model initialization time step, which had a value of 0.

2.3 WRF model

The WRF model used for the simulation was the Advanced Research WRF (WRF-ARW) model version 3.2.1 with the following physics configuration: WSM-3 class simple ice microphysics scheme (Hong et al., 2004), Dudhia shortwave radiation scheme (Dudhia, 1989), Rapid Radiative Transfer Model (RRTM) longwave radiation scheme (Mlawer et al., 1997), no cumulus parameterization, Medium-Range Forecast (MRF; Hong and Pan, 1996) PBL scheme, and the MM5 land surface scheme (Noah LSM).

GMDD
7, 2705–2743, 2014

The model was run on three nested domains using 1-way nesting (Fig. 2). The horizontal grid scales were the 36 km CONUS domain, 12 km eastern Texas domain, and the 4 km Houston–Galveston–Brazoria domain. All simulation results are taken from the 4 km domain at the grid point representing the UH Coastal Center (Fig. 1). Observational nudging was used in all runs and the model was initialized on 00:00 UTC 28 August 2006 and ended on 23:00 UTC 1 September 2006. Grid analysis was incorporated using North America Mesoscale (NAM) and United States Geological Survey (USGS) land surface data; observational analysis was incorporated using TCEQ CAMS sites for temperature and wind reanalysis.

2.4 MM5 model

In order to examine any improvements made from the MM5 to WRF simulations, data extracted from an MM5 simulation was used for a baseline comparison (Table 3). Similarily to previous studies by Ngan et al. (2012) for the TexAQS-II case, we applied MM5, version 3.6.1. The physics options included the MRF PBL scheme, Noah LSM, Grell cloud scheme (Grell and Devenyi, 2002), simple ice microphysics scheme, and RRTM radiation scheme. Observational nudging was used for these runs and was initialized with the Eta Data Assimilation System (EDAS) dataset (MM5E).

2.5 Differences between the WRF and MM5 configurations

The differences between the two models' configurations are the cloud scheme and the land analysis used for the initialization. While the WRF model has no cloud scheme, the MM5 model uses the Grell cloud scheme, which calculates an appropriate initial guess in combination with observations to use in predicting future convective activity. The EDAS and NAM land surface datasets are similar and use similar observational techniques for data interpolation, but the EDAS runs every three hours, which allows for higher-resolution temporal interpolation than the NAM data, which only runs every six hours (EDAS Archive Information, National Weather Service Environmental Center).

GMDD
7, 2705–2743, 2014

Using a more high-resolution dataset should lead to better first-guess and ongoing simulations in MM5.

2.6 Statistical analysis

2.6.1 Calculated statistics

For the purposes of this study, the coefficient of determination (r^2) and bias are displayed. The r^2 was calculated using a linear model in Matlab and the bias was determined by first calculating the perturbation from the observations, summing the values and dividing by the number of values:

$$\text{BIAS} = \frac{1}{n}\sum (Y' - Y) \quad (1)$$

where n is the number of values, Y' is the modeled value, and Y is the observed value.

2.6.2 Determination of additional statistic groups

Hourly values were collected from 00:00 CST 28 August–17:00 CST 1 September, resulting in 114 data points (Table 4). Biases and r^2 values were evaluated for the complete data set as well as for diurnal and frontal clusters. For the diurnal statistics, daytime referred to any data between 06:00 CST and 18:00 CST. Rappenglück et al. (2008) discussed the frontal passage that occurred during this period, which occurred during the evening of 29 August. An examination of the meteorology shows that generally southerly winds gave way to sustained northerly winds on 29 August around 18:30 CST, indicating this frontal passage. For the purposes of this study, the prefrontal period runs from 00:00 CST 28 August to 19:00 CST 29 August, and the postfrontal period runs from 20:00 CST 29 August to 17:00 CST 1 September.

GMDD
7, 2705–2743, 2014

3 Results and discussion

3.1 Standard meteorological variables

3.1.1 Temperature

WRF has the highest r^2 for all of the study period as well as when the data is separated into daytime, nighttime, prefrontal, and postfrontal time periods (Table 5). The largest differences between the WRF and MM5 model in the r^2 value occur at night and during prefrontal conditions, both of which have differences of 0.54. However, the nighttime r^2 value for MM5 was the smallest at 0.04, which reflects the variability in the nighttime temperature modeling. The WRF model has a higher nighttime r^2 value of 0.58, but this value also represents the smallest r^2 value for the model, which implies that both models have difficulty getting nighttime temperatures correct. Batching the data into prefrontal and postfrontal groups had little effect on the r^2 values for WRF, but led to increased values in both of the MM5 models.

WRF also has the smallest magnitude bias for the entire study period as well as for the daytime, nighttime, prefrontal period, and postfrontal period. The overall biases for all of the simulations are relatively low but both WRF and MM5 underestimate temperatures by about half a degree during the day and overestimate temperatures by about a degree at night for the entire study period (Table 5). These biases could possibly be attributed to too much moisture in the models, which would suppress temperature amplitudes. This warm nighttime bias is especially evident on the nights of 30 August and 31 August and is reflected in the increased post-frontal bias values (Fig. 3 and Table 5). These biases could be the product of too much moisture in the model, which would lead to less suppressed temperature peaks. Another possibility is that there is too much nighttime surface energy in the model, which could lead to increased nighttime temperatures. Also, higher modeled nighttime winds could lead to a well-mixed nighttime atmosphere, which would prevent temperatures from dropping as low as they should in the model.

GMDD
7, 2705–2743, 2014

Steeneveld et al. (2010) noted that both of the models have difficulty simulating nighttime temperatures. That same study also mentioned that the MM5 warming and cooling trends tended to lag behind the observations, which is visible in the time series for the first half of this study as well (Fig. 3). The WRF model simulation does not have this same time lag.

3.1.2 Water vapor

MM5 values were extracted at a lower precision, so both WRF and the observations were rounded to the same precision in order to make a fair comparison (not shown). However, the WRF r^2 values are again higher than the MM5 r^2 values (Table 5). The overall r^2 values were highest for both WRF and MM5. WRF had the highest overall and postfrontal values. Both of the models saw low r^2 values prior to the frontal passage, which increased following the frontal passage and more than doubled in the case of WRF. WRF had the highest postfrontal values but the lowest prefrontal values. The water vapor mixing ratio r^2 values are relatively high although they are lower than the temperature r^2 values. Daytime water vapor mixing ratio tended to be higher than the overall r^2, while nighttime water vapor r^2 values were slightly lower than the overall r^2 for both simulations. WRF overall, daytime, and nighttime r^2 values were higher than MM5, although this trend changes for the prefrontal and postfrontal conditions.

Table 5 shows that both models underestimated moisture for the entire study period with dry biases of 0.46 $g\,kg^{-1}$ and 2.61 $g\,kg^{-1}$ for WRF and MM5, respectively. During the day, this dry bias increases for both WRF and MM5 to 0.50 $g\,kg^{-1}$ and 2.81 $g\,kg^{-1}$. However, at night, the dry bias decreases to 0.40 $g\,kg^{-1}$ and 2.36 $g\,kg^{-1}$ for WRF and MM5, respectively. Zhong et al. (2007) modeled water vapor at the UH-CC and saw biases of 1.38 during the day, −0.63 at night, and 0.37 for the overall value, which indicated overestimation of moisture during the day and underestimation at night. The difference in the two models' moisture bias could be attributed to the different land initialization schemes used for the two models, but in either case temperature performance

GMDD
7, 2705–2743, 2014

during the entire study period appears to be affected by more than the water vapor mixing ratios.

For the two days following the frontal passage, the models' temperature and water vapor mixing ratio biases appear to be more coupled. WRF underestimates daytime temperature with a bias of 0.71 °C and could correspond to a moist bias of 0.5 g kg^{-1}, while MM5 slightly overestimates daytime temperature with a bias of 0.12 °C and could correspond to a dry bias of 2.05 g kg^{-1} (Table 5). The days following the frontal passage were mostly cloudless, so temperature may be more directly affected by moisture. The fact that following the frontal passage the conditions are more dry could also be a contributing factor, as the observed water vapor mixing ratio dropped by approximately 4 g kg^{-1} for the remainder of the study period (figure not shown). Moisture bias effects could be magnified in light of much smaller moisture values.

For the two nights following the frontal passage, both models' dry biases are relatively close to the mean nighttime biases of the entire study period, but temperature biases are not proportional to these changes. The nighttime biases decrease by only 0.04 g kg^{-1} and 0.09 g kg^{-1} for WRF and MM5, respectively, but both models clearly overestimate temperature on the nights of 30 August and 31 August (Fig. 3). For the entire study period, the models have too warm nighttime biases of 1.09 °C and 1.33 °C for WRF and MM5, respectively; these warm biases increase to 2.62 °C and 3.81 °C for those two nights.

3.1.3 Wind speed

Wind speeds had generally low r^2 values, with the highest overall r^2 being the MM5 simulation using EDAS (Fig. 3). Separating data into day and nighttime values did not increase the r^2 values; in fact, both day and nighttime r^2 were lower than the overall values for both of the models. While the MM5 model bias was relatively small and slightly underestimated during the daytime, the WRF model overestimated with a much higher magnitude. Both models have the largest biases at night when wind speeds are overestimated, and with the highest overestimation occurring by the WRF model. Ngan

GMDD
7, 2705–2743, 2014

et al. (2012) mention that modeled MM5 winds persisted for hours after the observed winds had died down at sunset. A similar trend is visible for a few nights of this study period in MM5, but is most clearly evident in the WRF model.

Wind speed r^2 values were equally low for both prefrontal and postfrontal conditions. However, clustering data by frontal condition led to having at least one higher r^2 value for each model than for all of the data combined (Table 5). In WRF3, the prefrontal value was higher than the postfrontal value, and this was the highest prefrontal value among the models. The MM5 model postfrontal value was higher. Prefrontal biases are low and then increase in the postfrontal environment, with WRF3 making a jump in overestimations following the front. Tucker et al. (2010) found that daytime winds tended to be higher and be more southerly following strong low level jet (SLLJ) nights, and they were weaker and either northerly or stagnant following weak LLJ (WLLJ) nights. Although it slightly overestimates wind speeds, WRF is able to better capture the post-SLLJ conditions on 28 August which correspond to prefrontal conditions. However, WRF persists in generating high winds on the days following two WLLJ nights (31 August and 1 September), which correspond to postfrontal conditions and leads to a much higher bias and lower r^2 values. The MM5 model does not suffer from high bias to the same extent, but it also tends to overestimate more following the postfrontal conditions corresponding to the post-WLLJ scenario.

3.1.4 Wind direction

Wind direction r^2 values were generally low for the entire study period and at nighttime for both models, and only reach approximately 0.50 during the daytime (Table 5). Houston's proximity to the Gulf generally means that there is a strong diurnal cycle as the temperature difference between the land and the water creates surface pressure gradients. This cycle tends to manifest itself in strong southerly winds during the daytime and more northerly winds in the evening and at night. However, during this time period the frontal passage led to more persistent northerly winds, which might have interfered with the normal cycle of the models (Fig. 3). The prefrontal and postfrontal r^2 values

GMDD
7, 2705–2743, 2014

are both very similarly low for both models with values at or near 0.30. During the study period, wind direction was variable as the front and the daytime wind cycle came into contact.

The magnitudes for the overall, daytime, and nighttime biases were an order of magnitude larger for WRF than for MM5. Wind direction for the entire study was underestimated by 22.57° and 2.41° in WRF and MM5, respectively, which means that the wind directions were in the same quadrant, but for WRF started having more of an orthogonal wind component. During the daytime these bias magnitudes increase for both models, although the MM5 model has a larger increase. This could possibly be related to the frontal passage, especially during the day when the frontal passage and the land–sea breeze cycle led to stagnant air conditions and wind directions were variable. Southerly winds are associated with moist, ocean air, while north and northwesterly winds are associated with drier, continental air, so the direction of the wind in the models could relate to the level of water vapor mixing ratio found in the models.

3.2 Energy budget variables

3.2.1 Radiation

Longwave outgoing radiation was only available at the top of the atmosphere for both WRF and MM5, creating a large bias for both of the models and not adequately capturing the values at the surface. Therefore this variable was removed from the study analysis, and only the other three components of radiation were studied (Table 5).

Incoming-longwave radiation

The r^2 values for longwave radiation are lower than for either temperature or water vapor mixing ratio, but are still relatively high (Table 5). WRF3 has a slightly higher r^2 during the daytime than overall, while MM5E is slightly lower than the overall value during the daytime. The overall and daytime WRF3 r^2 values are higher than the MM5E

GMDD
7, 2705–2743, 2014

values, but at night, MM5 has a slightly higher r^2 than the WRF model. Both models have relatively low nighttime r^2 values compared to either daytime or overall values.

Both models consistently overestimate incoming longwave radiation with the largest overestimations occurring at night. WRF consistently has larger biases than MM5. However, the minimum longwave radiation value recorded during this time period was $\sim 371\,\mathrm{W\,m^{-2}}$. Even the largest bias ($11\,\mathrm{W\,m^{-2}}$) only represents a 2 % overestimation of incoming longwave radiation.

There is a slight time lag in both the cooling and the warming trends for the longwave radiation for both models, but they both also attempt to capture the drop in radiation following the frontal passage (Fig. 4). Both of the models overestimated; prefrontal conditions produced the largest bias. In WRF there is an almost 30 % drop in bias from the prefrontal to postfrontal data cluster, and a 50 % drop for the MM5 model. MM5E had the lowest overall and frontal cluster biases, while WRF had the highest total and postfrontal values.

Incoming/outgoing shortwave radiation

Although the relationship between incoming and outgoing shortwave radiation is not one-to-one, the models tend to treat outgoing radiation as a direct decrease caused by albedo. Therefore, both incoming and outgoing shortwave radiation are driven to 0 after sunset, leading to the "not a number" (NaN) values found in the tables for nighttime values. For outgoing radiation, the WRF model performs better than the MM5 model, which has very small r^2 values during the daytime (Table 5). These small r^2 values are most likely the result of the overestimations found during the early part of the study period when MM5 overestimates outgoing shortwave radiation by as much $337\,\mathrm{W\,m^{-2}}$ (Fig. 4) and results in daytime biases of $60\,\mathrm{W\,m^{-2}}$. While the overall bias in the WRF model is slightly underestimated, it is overestimated in MM5 with a magnitude of $33\,\mathrm{W\,m^{-2}}$.

GMDD
7, 2705–2743, 2014

For the first two days of the study period, incoming solar radiation (SWDOWN) did not reach maximum insolation peaks, possibly due to scattered cloud cover. Following the frontal passage on 29 August, cloud cover began to dissipate as observed incoming solar radiation began to increase, reaching maximum insolation on the afternoon of 31 August before again devolving on 1 September. However, both models moved too soon in developing maximum insolation (Fig. 4).

During the daytime for the entire study period, WRF tended to underestimate SWDOWN while MM5 tended overestimate (Table 5). However, for the two clearest days of the study period, both WRF and MM5 overestimated incoming solar radiation by 51.9 $W m^{-2}$ and 52.9 $W m^{-2}$, respectively. While these values drop to 11.53 $W m^{-2}$ and 17.27 $W m^{-2}$ on the clearest day of the study, both models continue to overestimate incoming solar radiation. This excess energy in the models could appear as overestimations in the energy flux partitions for sensible, latent, and ground flux.

Incoming radiation r^2 values are generally higher than the outgoing values for both of the models, but daytime r^2 values are still lower than the overall r^2 values (Table 5). WRF performs better than the MM5 model for all values. Again, WRF tends to underestimate the radiation while the MM5 model overestimates, but the magnitudes of the biases for incoming radiation are smaller, only reaching a maximum magnitude of 24 $W m^{-2}$ (Table 5). Similar to outgoing radiation, the magnitude of the daytime biases is higher than either the overall biases or nighttime biases.

For both outgoing and incoming radiation, daytime r^2 values and biases could be affected by the delayed onset of daytime radiation in the models. Both models take an additional hour before seeing increased incoming and outgoing solar radiation values, which is especially visible following the frontal passage (Fig. 4). The averaging of the hourly observations when sunrise occurred in the middle of an hour may also contribute to the discrepancy between the observations and simulations. Incoming solar radiation has much smaller biases. The maximum daytime values reached 979 $W m^{-2}$, leading to a maximum daytime average bias of only 1 %.

GMDD
7, 2705–2743, 2014

The nighttime data, in part, contributes to the increase in overall high r^2 of both incoming and outgoing radiation when compared to the daytime values of the variables. Having this underestimation of daytime solar insolation could explain the cool bias in the WRF model, but does not explain the cool bias in the MM5 model.

Similar to the outgoing shortwave radiation, both models runs for incoming shortwave radiation have larger postfrontal r^2 values (Table 5). Both of the models have comparable r^2 values within frontal clusters, but the biases vary. Both of the models underestimated prior to the front and overestimated following the front, and the largest magnitude bias varied by model. WRF had the largest bias in the prefrontal cluster, while both MM5 models had larger bias in the postfrontal cluster.

3.2.2 Flux variables

Latent heat flux

The overall latent heat flux r^2 values for both simulations are even higher than for temperature, but decrease when considering the daytime values and become almost negligible when considering the nighttime values (Fig. 5). WRF3 again has the highest r^2 values for all of the groupings. When looking at the frontal passage period, the data tends to have a higher r^2 during the post-frontal period (Table 6).

The magnitudes of all of the model biases are much higher than those seen for any of the radiation values. The MM5 model has a larger bias magnitude than the WRF model with maximum magnitude bias of 65 $\mathrm{W\,m^{-2}}$ and 30 $\mathrm{W\,m^{-2}}$, respectively. The maximum daytime latent heat flux value was only 470 $\mathrm{W\,m^{-2}}$, which meant an 8 % decrease from the largest bias in MM5 to the bias in WRF. Overall and daytime latent heat flux is overestimated for both of the models with the largest biases occurring during the daytime. The nighttime biases for both of the models are relatively small and are underestimated in both models.

Prior to the frontal passage on 29 August, latent heat values were scattered throughout the day, which could correspond to lower moisture content (Fig. 5). Following the

GMDD
7, 2705–2743, 2014

frontal passage (30 and 31 August), observed daytime latent heat flux increases, indicating increased moisture. Both models overestimate daytime latent heat flux for the entire study period, but MM5 has larger overestimations than WRF by approximately 20 $W m^{-2}$ (Table 6). However, on 30 and 31 August both models perform similarly with overestimation biases of $\sim 41 W m^{-2}$ and $\sim 47 W m^{-2}$ for WRF and MM5, representing a difference of only 6 $W m^{-2}$. Both models vary in their simulation of the meteorological conditions prior to the frontal passage but resort to similar parameterizations following the front, perhaps in response to the these clearer incoming solar radiation simulations.

Sensible heat flux

MM5 has higher overall, daytime, and nighttime values of r^2 compared to WRF (Table 6). Both of the models had higher overall values compared to daytime clustering, while the nighttime values are low. Compared to the diurnal r^2, the r^2 is higher both for all data and for the prefrontal and postfrontal clusters (Table 6).

For the study period there was an r^2 value of 0.49 between observed sensible heat flux and water vapor mixing ratio at night. None of the models reach this level of r^2 values, but the MM5 models get closer to this relationship than the WRF model. This relationship may relate to the fact that for overall, daytime, and nighttime r^2, the MM5 models perform better than the WRF model. The decrease in r^2 from sensible heat flux to latent heat flux and the decrease in the magnitude of the biases are in agreement with the findings of Zhong et al. (2007). However, they do not agree with LeMone et al. (2009), who found that their modeled sensible heat overestimated throughout the entire study period and tended to have a larger bias than latent heat.

WRF3 had the highest overall and nighttime biases and MM5E had the highest daytime biases. WRF3 underestimated sensible heat flux for all clusters and MM5E underestimated only at night. While the r^2 decreased for sensible heat flux compared to latent heat flux and the biases are smaller, the relative magnitude of the biases represents a larger portion of measured values. During the daytime, MM5 had an average overestimation of 32 % while WRF underestimated by 28 %. This is only a 4 % disparity

GMDD
7, 2705–2743, 2014

between the values during the daytime, but this gap increases greatly at night, when WRF underestimated values by as much as 50 % while MM5 was only 2.4 %.

The sensible heat flux shows similar simulation pattern to the latent heat flux time series (Fig. 5). During the first two days of the study period, both models respond differently to the inconsistent sensible heat flux, but have very similar responses during the two days following the frontal passage. The initial variations in response seem to lead to disparate biases over the course of the study period, with daytime biases being overestimated by MM5 and being underestimated by WRF (Table 6). Sensible heating is associated with ground heating, so it is possible that temperature variations in the models, combined with differences in the moisture, could contribute to these variations. However, the two days following the frontal passage produce similar model responses, with WRF and MM5 overestimating sensible heat by $\sim 14\,\mathrm{W\,m^{-2}}$ and $6\,\mathrm{W\,m^{-2}}$, respectively.

Ground flux

Similar to the other flux variables, the overall r^2 values were higher than either the day or nighttime values (Table 6). Out of all the flux variables, the overall and daytime r^2 values for ground flux are the lowest. The nighttime r^2 values are also very low, but are higher than for either sensible or latent heat flux. The WRF model has slightly lower r^2 values than either of the MM5 models overall and during the day, but is slightly higher at night.

The ground flux biases do not follow the pattern of sensible and latent heat flux (Table 6). During the day both models consistently underestimate for the entire study period as well as for the two days following the frontal passage, and at night both models have similar overestimations. Additionally, both models have similar timing of the ground flux that lies in contrast with the observations (Fig. 5). Both models have sharp increases of ground flux in the evening that eventually diminish as the night progresses, while the observations have gradual increases in ground flux through the afternoon and then sharp drops in the morning. The ground flux is associated with increased ground

GMDD
7, 2705–2743, 2014

temperatures as the sun reaches the ground, so the increased insolation on the two days following the frontal passage leads to higher observed ground flux amplitudes. Both of the models capture these higher ground flux values, but have higher amplitudes of both the amount of ground flux escaping from and entering the ground, which again could be associated with the increased incoming solar radiation found in the models.

As a first approximation of the energy budget at the surface, the sum of these three flux variables' daytime biases, while accounting for the direction of each component, should equal the bias found in incoming solar radiation. On mostly cloudless days like 30 August and 31 August, the sum of the biases should be close to 50 $W m^{-2}$ for both models (Table 6). However, neither model comes close to this value: the sum of sensible, latent, and ground flux daytime biases for these two days was only $\sim 2\,W m^{-2}$ and $\sim -2\,W m^{-2}$ for WRF and MM5, respectively. Despite the fact that on the most cloudless day of the study period there is only an overestimation of less than 20 $W m^{-2}$ for both models, the sum of sensible, latent, and ground flux still does not approach this value for either model. These variables cannot completely account for the energy output in the models, so the rest of this energy might present itself in temperature or other increases during the daytime. On the other hand, a sum of the nighttime biases following the front yield values closer to the missing 50 $W m^{-2}$, which may imply that the models use latent, sensible, and ground heat fluxes as a reservoir to drive nighttime energy changes.

3.2.3 Turbulence

Friction velocity, or u^*, is one measure of how much turbulence is being generated through shearing forces at any given time (Stull, 1988). Examining the observed and modeled and measured values can provide insight into shear turbulence that contributes to the development of the PBL. Table 6 presents the overall and diurnal r^2 and bias values for friction velocity and Fig. 6 shows the time series for the study period.

GMDD
7, 2705–2743, 2014

Despite the fact that friction velocity is a small component of turbulent energy, the models are able to model it relatively well with overall r^2 values of 0.77 and 0.70 for WRF and MM5, respectively. The overall r^2 values for both of the models are higher than daytime values and much higher than the nighttime values. At night, the models are set to a minimum value of 0.1 $m s^{-1}$, which does not always accurately reflect the observations that can get much smaller. Above this threshold, both models attempt to mimic nighttime u^* behavior, but following the frontal passage, nighttime wind speeds were relatively calm (Fig. 3). On those nights observed u^* values were well below the 0.1 $m s^{-1}$ threshold, so neither model is able to simulate these values, which could have led to the low nighttime r^2 values.

Both models overestimate u^*, which could be related to the overestimations in wind speed for the models. There is no distinct cluster with the highest bias magnitudes; the largest bias for WRF3 occurs during the daytime but for MM5 occurs at night. WRF3 has the highest overall, daytime, and nighttime magnitude biases, which is in contrast with Hanna et al. (2010), who mentioned that MM5 had larger biases in the afternoon than WRF. Friction velocity is a measure of how much shear turbulence will be generated and is affected by topography and is directly related to wind speed. Compared to the other model variables, the absolute biases for friction velocity are relatively small, but assuming a maximum u^* value of approximately 0.6 $m s^{-1}$, the bias can be overestimated by nearly 15 % in the WRF model.

3.3 Planetary boundary layer

Due to the small number of radiosonde launches available for the duration of the study period, the biases were not calculated for planetary boundary layer height. However, PBL heights were calculated at sunrise and sunset prior to the frontal passage, and then following the frontal passage were recorded with more regularity, so the few observations available offer a better chance to look at the development and destruction of the PBL (Fig. 7). Ideally, suppressed daytime temperatures and elevated nighttime temperatures should yield similar PBL height results. However, while the daytime PBL

GMDD
7, 2705–2743, 2014

heights are in fact underestimated during the day as expected, they are also underestimated at night when they should be overestimated. Daytime peaks are better approximated following the frontal passage, but the PBL destruction always happens too soon.

There are various reasons for the possible variations in the onset of PBL development and destruction. Especially during the morning PBL height estimates, the late onset of solar radiation in the models could contribute to the slow development of the PBL during a time when convection leads to a rapid increase of PBL height. LeMone et al. (2009) suggests overestimations of sensible heat lead to overestimations in the convective boundary layer depth. The converse could apply in this study, where underestimations in sensible heat flux leads to underestimations in the PBL height simulations. In general, MM5E tends to overestimate sensible heat flux and generally has the smallest underestimations and largest overestimations, while WRF tends to substantially underestimate sensible heat and generally has lower PBL height estimations. However, a different PBL scheme was used; examining other PBL schemes to see if this trend is sustained could be beneficial.

Rappenglück et al. (2008) speculated whether PBL development was slower on ozone exceedance due to cooler temperatures delaying PBL development. In the post-frontal environment temperatures were in fact cooler (Fig. 3), but none of the models were able to simulate temperature minimums for the nights of 30 or 31 August. WRF gets closest to the simulated temperatures while MM5 has a larger bias following the front, which may explain why the models overestimated noontime PBL height on 30 August–1 September (Fig. 7). Increased PBL height allows for lower ozone concentrations, so it is no surprise that using MM5 simulations as a meteorological driver for air quality modeling led to underestimation of ozone on 31 August and 1 September by 25–30 ppb (Banta et al., 2011; Ngan et al., 2012).

GMDD
7, 2705–2743, 2014

4 Conclusions

Although WRF does not perform as well as MM5 in predicting PBL heights, it does a better job in capturing most of the general and energy budget variables. Energy balance partitioning can have an effect on standard and planetary boundary layer height variables. Both models overestimate incoming solar radiation, which implies a surplus of energy that could be exhibited in either the partitioning of the surface energy variables or in some other aspect of the meteorological modeling not examined here. At least following the frontal passage, some evidence suggested that this energy shows up in nighttime partitioning, in which case the sensible, latent, and ground fluxes are only discharging part of the energy during the daytime, which would lead to lower daytime temperatures. The WRF model's suppressed daytime temperatures would seem to confirm this scenario, but MM5 overestimates temperature on both of these days. This scenario would also imply that there is more energy available for the nighttime system, which should mean increased temperatures and higher boundary layer height estimations. While nighttime temperatures do seem to reflect this increased energy, PBL height estimations do not reflect it.

The nighttime temperature bias disparity in the models following the frontal passage could reflect the disparity in moisture. The MM5 model consistently had much drier conditions than the WRF model, which could mean more energy available to other parts of the meteorological system. On the clearest day of the study period MM5 had increased latent heat flux, which could lead to higher evaporation rates and lower moisture in the model. However, this latent heat disparity between the two models is not visible during any other part of the study, so examining sequential cloud-free days would be necessary to see whether the moisture and latent heat effect was sustained. The full effects of moisture on the energy balance cannot be determined here other than as a potential reason for inconsistent model outputs. The difference in the land datasets used to initialize and update each model make this situation plausible.

GMDD
7, 2705–2743, 2014

The frontal passage allowed this study to examine these variables both under prefrontal and postfrontal conditions, and it was found that a frontal passage does affect the performance of most of the variables, including the radiation, flux, and turbulence variables, at times creating significant differences in the r^2 values. Ultimately the clear, sunny days offered the most insight into the potential effects of the energy balance variables on standard variables and planetary boundary layer height. These two days were also two of the highest 8 h ozone peak days on record for the year. Since these kinds of days are favorable for high ozone production, the energy balance variables reproduced on these days could more accurately represent meteorological conditions. Accurately determining the energy balance variables could in turn produce better standard meteorology and PBL heights, which are essential in determining accurate ozone concentrations.

Acknowledgements. We are grateful for financial and infrastructural support provided by the UH-CC and we like to thank Fong Ngan (NOAA-ARL) for valuable discussions.

References

Air Resources Laboratory: Eta Data Assimilation System (EDAS) Archive Information, available at: http://ready.arl.noaa.gov/edas80.php (last access: 2 December 2013), 2013.

Banta, R. M., Senff, C., Nielsen-Gammon, J., Darby, L., Ryerson, T., Alvarez, R., Spandberg, S., Williams, E., and Trainer, M.: A bad air day in Houston, B. Am. Meteorol. Soc., 86, 657–669, 2005.

Banta, R. M., Senff, C., Alvarez, R., Langford, A., Parrish, D., Trainer, M., Darby, L., Hardesty, R., Lambeth, B., Neuman, J., Angevine, W., Nielsen-Gammon, J., Sandberg, S., and White, A.: Dependence of daily peak O_3 concentrations near Houston, Texas on environmental factors: wind speed, temperature, and boundary-layer depth, Atmos. Environ., 45, 162–173, 2011.

Borge, R., Alexandrov, V., del Vas, J. J., Lumbreras, J., and Rodriguez, E.: A comprehensive sensitivity analysis of the WRF model for air quality applications over the Iberian Peninsula, Atmos. Environ., 42, 8560–8574, 2008.

GMDD

7, 2705–2743, 2014

Byun, D. W. and Schere, K.: Review of the governing equations, computational algorithms, and other componenets of the Models-3 community multiscale air quality (CMAQ) modeling system, Appl. Mech. Rev., 59, 51–77, 2006.
Chen, F. and Dudhia, J.: Coupling an advanced land surface hydrology model with the Penn State-NCAR MM5 modeling system. Part 1: Model implementation and sensitivity, Mon. Weather Rev., 129, 569–585, 2001.
Clements, C. B., Zhong, S., Goodrick, S., Li, J., Potter, B. E., Bian, X., Heilman, W. E., Charney, J. J., Perna, R., Jang, M., Lee, D., Patel, M., Street, S., and Aumann, G.: Observing the dynamics of wildland grass fires – FireFlux – a field validation experiment, B. Am. Meteorol. Soc., 88, 1369–1382, 2007.
Day, B. M., Rappenglück, R., Clements, C., Tucker, S., and Brewer, W.: Nocturnal boundary layer characteristics and land breeze development in Houston, Texas during TexAQS II, Atmos. Environ., 44, 4014–4023, 2010.
Dudhia, J.: Numerical study of convection observed during the winter monsoon experiment using a mesoscale two-dimensional model, J. Atmos. Sci., 46, 3077–3107, 1989.
Gilliam, R. and Pleim, J.: Performance assessment of new land surface and planetary boundar layer physics in the WRF-ARW, J. Appl. Meteorol. Clim., 49, 760–774, 2010.
Grell, G. A. and Devenyi, D.: A generalized approach to parameterizing convection combining ensemble and data assimilation techniques, Geophys. Res. Lett., 29, 38.1–38.4, doi:10.1029/2002GL015311, 2002.
Grell, G. A., Dudhia, J., and Stauffer, D.: A description of the fifth-generation Penn State/NCAR Mesoscale Model (MM5), NCAR Tech. Note NCAR/TN-3981STR, 122 pp., 1994.
Hanna, S. R., Reen, B., Hendrick, E., Santos, L., Stauffer, D., Deng, A., McQueen, J., Tsudulko, M., Janjic, Z., Jovic, D., and Sykes, R.: Comparison of observed, MM5, and WRF-NMM model-simulated, and HPAC-assumed boundary layer meteorological variables for 3 days during the IHOP field experiment, Bound.-Lay. Meteorol., 134, 285–306, 2010.
Hong, S. Y. and Pan, H. L.: Nonlocal boundary layer vertical diffusion in a medium range-forecast model, Mon. Weather Rev., 124, 2322–2339, 1996.
Hong, S. Y., Dudhia, J., and Chen, S. H.: A revised approach to ice microphysical processes for the bulk parameterization of clouds and precipitation, Mon. Weather Rev., 132, 103–120, 2004.
Hu, X. M., Nielsen-Gammon, J., and Zhang, F.: Evaluation of three planetary boundary layer schemes in the WRF model, J. Appl. Meteorol. Clim., 49, 1831–1844, 2010.

GMDD
7, 2705–2743, 2014

Langford, A. O., Tucker, S., Senff, C., Banta, R., Brewer, W., Alvarez, R., Hardesty, R., Lerner, B., and Williams, E.: Convective venting and surface ozone in Houston during TexAQS2006, J. Geophys. Res., 115, D16305, doi:10.1029/2009JD013301, 2010.

LeMone, M., Chen, F., Tewari, M., Dudhia, J., Geerts, B., Miao, Q., Coulter, R., and Grossman, R.: Simulating the IHOP_2002 fair-weather CBL with the WRF-ARW-Noah modeling system. Part 1: Surface fluxes and CBL Structure and evolution along the eastern track, Mon. Weather Rev., 138, 722–744, 2009.

Mao, Q., Gautney, L. L., Cook, T. M., Jacobs, M. E., Smith, S. N., and Kelsoe, J. J.: Numerical experiments MM5-CMAQ sensitivity to various PBL schemes, Atmos. Environ., 40, 3092–3110, 2006.

Mlawer, E. J., Taubman, S., Brown, P., Iacono, M., and Clough, S.: Radiative transfer for inhomogeneous atmosphere: RRTM, a validated correlated-*k* model for the longwave, J. Geophys. Res., 102, 16663–16682, 1997.

National Weather Service Environmental Modeling Center: NAM: the North American Mesoscale Forecast System, available at: http://www.emc.ncep.noaa.gov/index.php?branch=NAM (last access: 24 November 2013), 2013.

Ngan, F. and Byun, D.: Classification of weather patterns and associated trajectories of high-ozone episodes in the Houston–Galveston–Brazoria area during the 2005/06 TexAQS-II, J. Appl. Meteorol. Clim., 50, 485–499, 2011.

Ngan, F., Byun, D., Kim, H. C., Lee, D. G., Rappenglück, B., and Pour-Biazar, A.: Performance assessment of retrospective meteorological inputs for use in air quality modeling during TexAQS 2006, Atmos. Environ., 54, 86–96, 2012.

Rappenglück, B., Perna, R., Zhong, S., and Morris, G.: An analysis of the vertical structure of the atmosphere and the upper-level meteorology and their impact on surface ozone levels in Houston, Texas, J. Geophys. Res., 113, D17315, doi:10.1029/2007JD009745, 2008.

Skamarock, W. C., Klemp, J., Dudhia, J., Gill, D., Barker, D., Duda, M., Hwang, X. Y., and Powers, J.: A Description of the Advanced Research WRF Version 3, NCAR Tech Note NCAR/TN-4751STR, UCAR Communications, Boulder, CO, 125 pp., 2008.

Steenveld, G. J., Wokke, M., Zwaaftink, C., Pijlman, S., Heusinkveld, B., Jacobs, A., and Holtslag, A.: Observations of the radiation divergence in the surface and its implication for its parameterization in numerical weather prediction models, J. Geophys. Res., 115, D06107, doi:10.1029/2009JD013074, 2010.

GMDD
7, 2705–2743, 2014

Stull, R. B.: An Introduction to Boundary Layer Meteorology, 13th edn., Atmospheric and Oceanographic Sciences Library, Springer Publishers, 1988.

Tucker, S. C., Banta, R., Langford, A., Senff, C., Brewer, W., Williams, E., Lerner, B., Osthoff, H., and Hardesty, R.: Relationships of coastal nocturnal boundary layer winds and turbulence to Houston ozone concentrations during TexAQS 2006, J. Geophys. Res., 115, D10304, doi:10.1029/2009JD013169, 2010.

Wilczak, J. M., Djalalova, I., McKeen, S., Bianco, L., Bao, J. W., Grell, G., Peckham, S., Mathur, R., McQueen, J., and Lee, P.: Analysis of regional meteorology and surface ozone during the TexAQS II field program and an evaluation of the NMM-CMAQ and WRF-Chem air quality models, J. Geophys. Res., 114, D00F14, doi:10.1029/2008JD011675, 2009.

Zhong, S., In, H. J., and Clements, C.: Impact of turbulence, land surface, and radiation parameterizations on simulated boundary layer properties in a coastal environment, J. Geophys. Res., 112, D13110, doi:10.1029/2006JD008274, 2007.

GMDD

7, 2705–2743, 2014

Table 1. Variable names and descriptions for the study.

Variable Name (Units)	Description
TEMP2 (°C)	Temperature at 2 m
Q2 ($g kg^{-1}$)	Water vapor mixing ratio at 2 m
WSPD10 ($m s^{-1}$)	Wind speed at 10 m
WDIR10 (°)	Wind direction at 10 m
LHFLUX ($W m^{-2}$)	Latent heat flux at surface
SHFLUX ($W m^{-2}$)	Sensible heat flux at surface
GRNDFLUX ($W m^{-2}$)	Ground flux at surface
SWDOWN ($W m^{-2}$)	Shortwave incoming radiation at surface
LWDOWN ($W m^{-2}$)	Longwave incoming radiation at surface
SWUP ($W m^{-2}$)	Shortwave outgoing radiation at surface
USTAR ($m s^{-1}$)	Friction velocity
PBLH (m)	Planetary boundary layer height

GMDD
7, 2705–2743, 2014

Table 2. Radiosonde launch times (CST).

27 Aug 2006	28 Aug 2006	29 Aug 2006	30 Aug 2006	31 Aug 2006	1 Sep 2006
18:00	06:00	06:00	06:00	04:00	04:00
	18:00	18:00	12:00	06:00	06:00
			18:00	09:00	09:00
				12:00	12:00
				15:00	15:00
				18:00	
				21:00	
Total # Radiosondes: 20					

GMDD
7, 2705–2743, 2014

Table 3. Model simulation configurations.

Simulation	Model	PBL Scheme	LSM	Land Analysis
MM5E	MM5	MRF	Noah	EDAS
WRF3	WRF-ARW	MRF	Noah	NAM

GMDD
7, 2705–2743, 2014

Table 4. Data clusters.

Cluster	Number Data Points
All	114
Daytime	64
Nighttime	50
Prefrontal	44
Postfrontal	77

GMDD
7, 2705–2743, 2014

Table 5. Results for r^2 and bias for all, diurnal, and frontal conditions for temperature (TEMP2), water vapor mixing ratio (Q2), wind speed (WSPD10), wind direction (WDIR), incoming longwave radiation (LWDOWN), Outogoing shortwave radiation (SWUP), and incoming shortwave radiation (SWDOWN).

	TEMP2		Q2		WSPD10		WDIR10		LWDOWN		SWUP		SWDOWN	
	WRF3	MM5E	WRF3	MM5E	WRF3	MM5E	WRF3	MM5E	WRF3	MM5E	WRF3	MM5E	WRF3	MM5E
r^2	0.87	0.56	0.80	0.74	0.36	0.40	0.34	0.29	0.68	0.64	0.79	0.52	0.82	0.81
r^2_Day	0.86	0.48	0.81	0.78	0.33	0.31	0.49	0.50	0.73	0.61	0.60	0.23	0.66	0.64
r^2_Night	0.58	0.04	0.77	0.69	0.04	0.45	0.10	0.03	0.41	0.47	NaN	NaN	NaN	NaN
r^2_Prefront	0.90	0.36	0.30	0.38	0.68	0.18	0.30	0.30	0.64	0.45	0.66	0.65	0.68	0.64
r^2_Postfront	0.88	0.65	0.65	0.57	0.55	−0.11	0.30	0.27	0.49	0.48	0.90	0.76	0.93	0.92
Bias	0.19	0.23	−0.46	−2.61	0.86	0.54	−22.57	−2.41	9.59	3.00	−2.32	33.23	−13.92	9.56
Bias_Day	−0.52	−0.62	−0.50	−2.81	0.27	−0.08	−26.17	−8.32	8.51	2.76	−2.84	60.49	−24.78	17.04
Bias_Night	1.09	1.33	−0.40	−2.36	0.94	0.34	−17.97	5.17	10.97	3.30	−1.66	−1.66	−0.01	−0.01
Bias_Prefront	−0.34	−0.73	−0.70	−2.77	0.36	0.40	3.48	−10.23	11.66	4.35	−11.21	79.12	−61.57	−24.00
Bias_Postfront	0.52	0.84	−0.30	−2.51	0.33	0.31	−38.95	2.51	8.29	2.15	3.26	4.38	16.03	30.65

GMDD
7, 2705–2743, 2014

Table 6. Results for r^2 and bias for all, diurnal, and frontal conditions for latent heat flux (LHFLUX), sensible heat flux (SHFLUX), ground flux (GRNDFLUX), and friction velocity (USTAR).

	LHFLUX		SHFLUX		GRNDFLUX		USTAR	
	WRF3	MM5E	WRF3	MM5E	WRF3	MM5E	WRF3	MM5E
r^2	0.90	0.87	0.73	0.77	0.66	0.67	0.77	0.70
r^2_Day	0.80	0.75	0.59	0.64	0.46	0.47	0.66	0.56
r^2_Night	0.15	0.00	0.00	0.16	0.20	0.13	0.11	0.11
r^2_Prefront	0.80	0.75	0.57	0.71	0.57	0.60	0.76	0.61
r^2_Postfront	0.94	0.92	0.85	0.81	0.71	0.70	0.79	0.77
Bias	16.37	26.99	−5.16	3.75	−2.01	−4.63	0.06	0.02
Bias_Day	29.63	49.84	−5.77	6.83	−15.68	−14.98	0.08	0.01
Bias_Night	−0.61	−2.27	−4.37	−0.21	15.49	8.62	0.04	0.03
Bias_Prefront	5.12	16.46	−14.02	5.39	−1.58	−1.99	0.04	0.00
Bias_Postfront	23.44	33.61	0.41	2.71	−2.28	−6.29	0.07	0.02

GMDD
7, 2705–2743, 2014

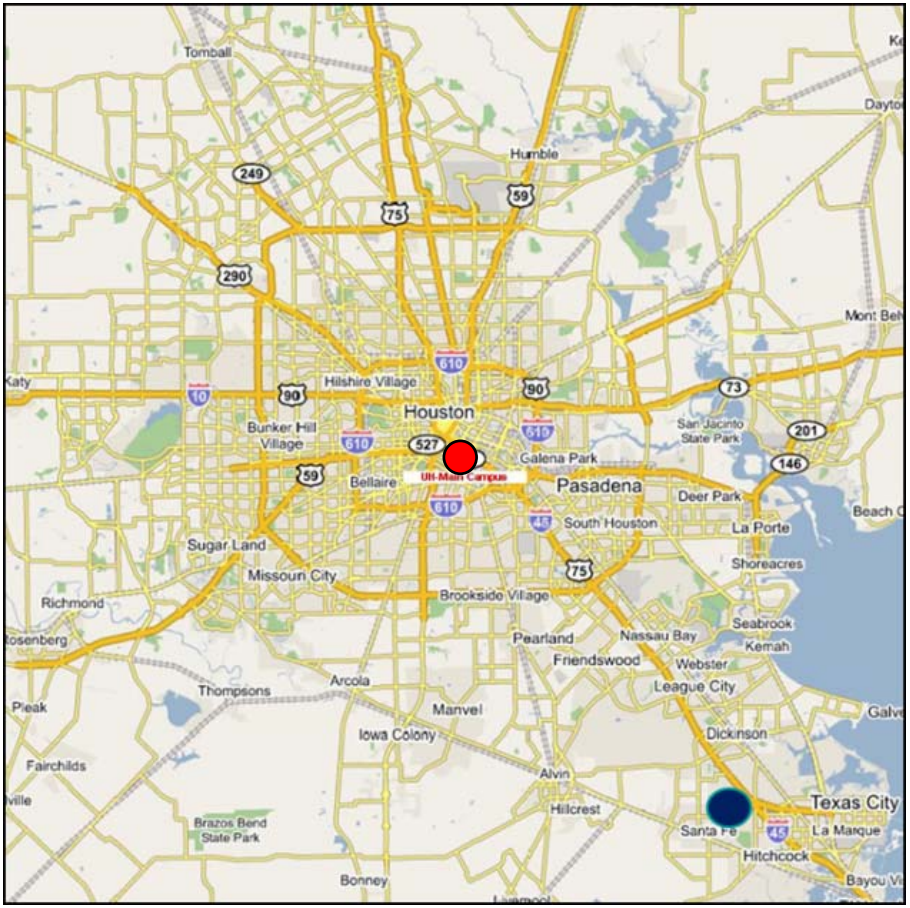

Fig. 1. Location of model and measurements. The dark blue dot represents the UH Coastal Center and the red dot represents the UH Main Campus where the radiosondes were launched.

GMDD
7, 2705–2743, 2014

MM5 v3.6.1 and WRF v3.2.1 model comparison

C.-S. M. Wilmot et al.

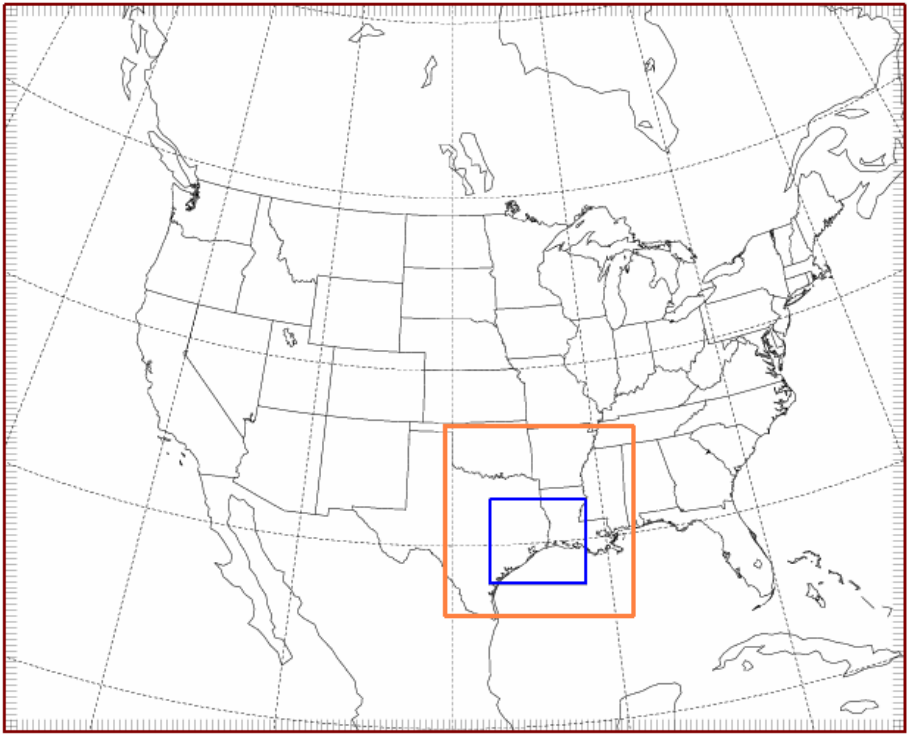

Fig. 2. Nesting domain for WRF model. The blue box is the 4 km domain that all model outputs were extracted from.

GMDD
7, 2705–2743, 2014

MM5 v3.6.1 and WRF v3.2.1 model comparison

C.-S. M. Wilmot et al.

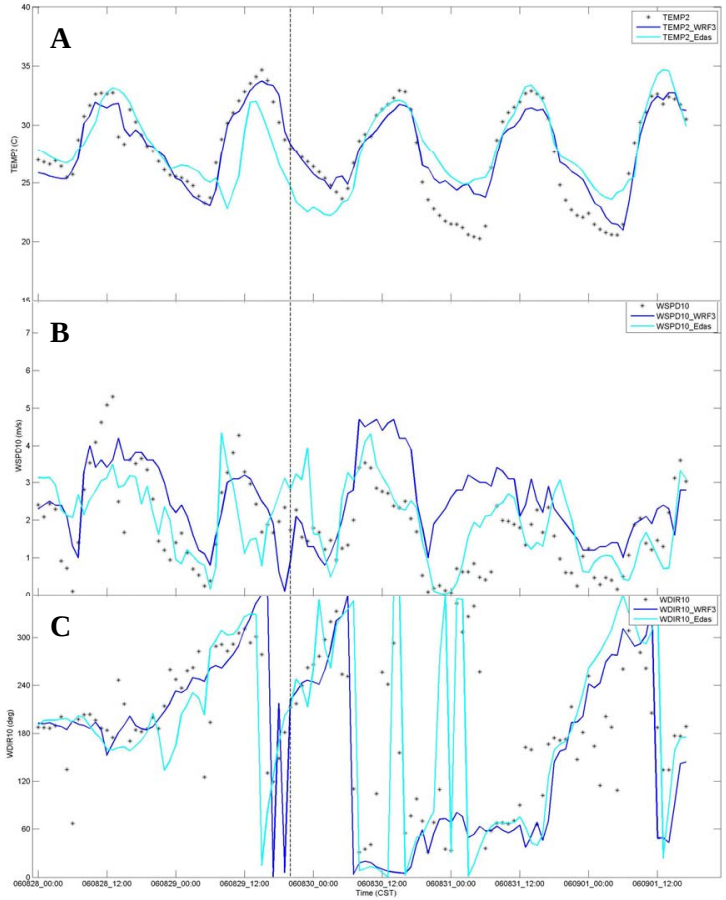

Fig. 3. Time series of temperature **(A)**, wind speed **(B)**, and wind direction **(C)** for observations (dots) and for the WRF (blue) and MM5 with EDAS (green) models. The dotted line marks the beginning of postfrontal conditions.

GMDD
7, 2705–2743, 2014

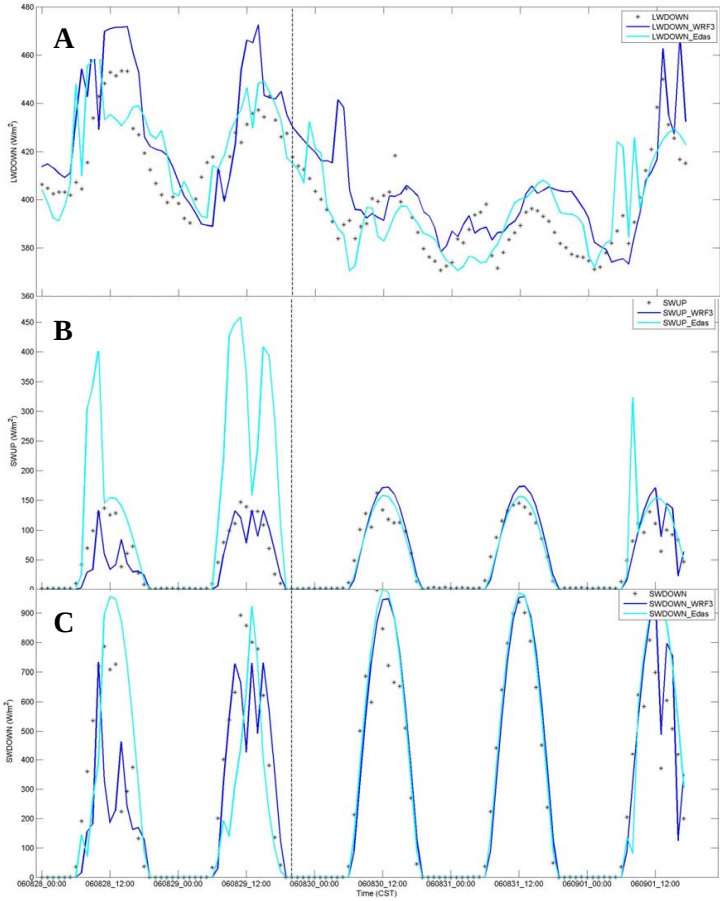

Fig. 4. Time series for incoming longwave **(A)**, outgoing shortwave **(B)**, and incoming shortwave **(C)** radiation for observations (dots) and for the WRF (blue) and MM5 with EDAS (green) models.

GMDD
7, 2705–2743, 2014

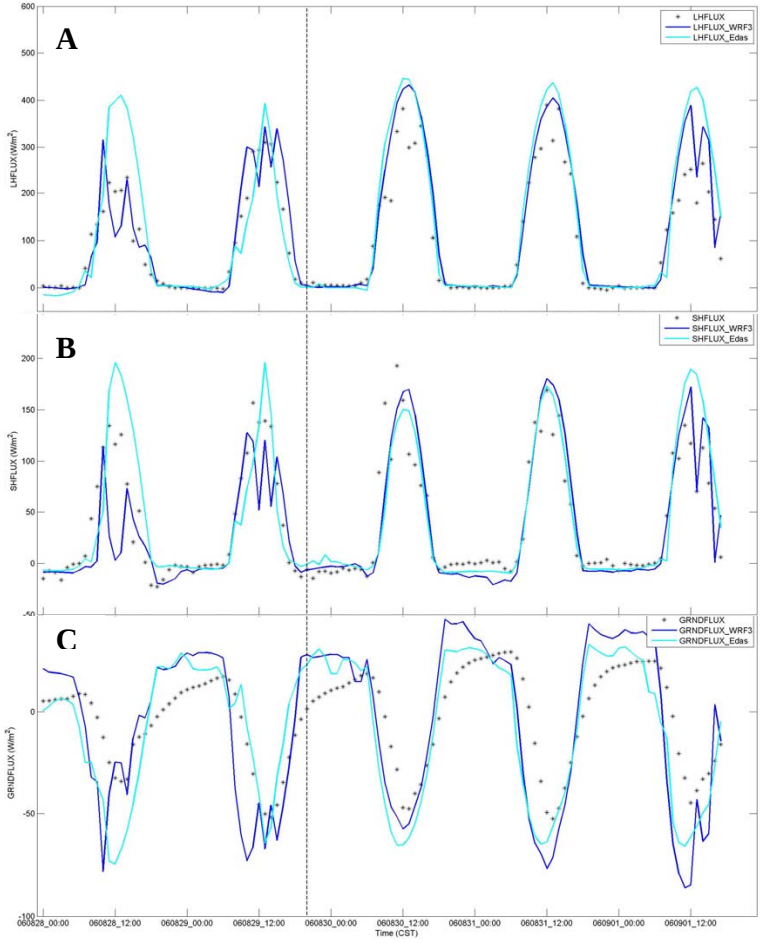

Fig. 5. Time series for latent heat **(A)**, sensible **(B)**, and ground **(C)** flux for observations (dots) and for the WRF (blue) and MM5 with EDAS (green) models.

GMDD
7, 2705–2743, 2014

MM5 v3.6.1 and WRF v3.2.1 model comparison

C.-S. M. Wilmot et al.

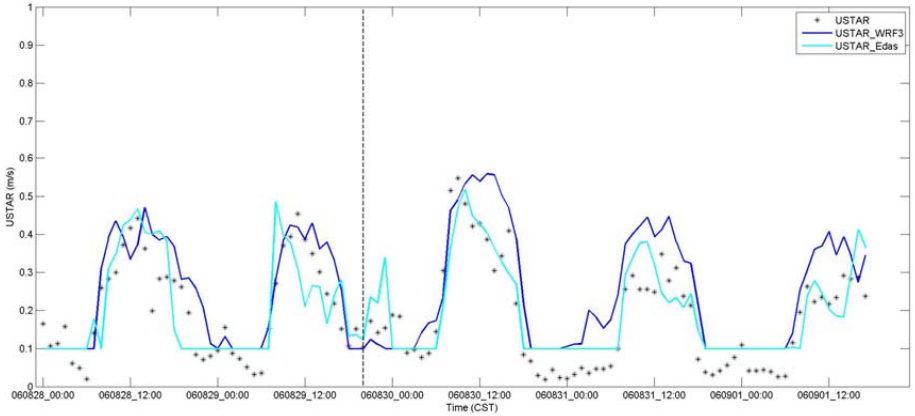

Fig. 6. Time series for friction velocity.

GMDD
7, 2705–2743, 2014

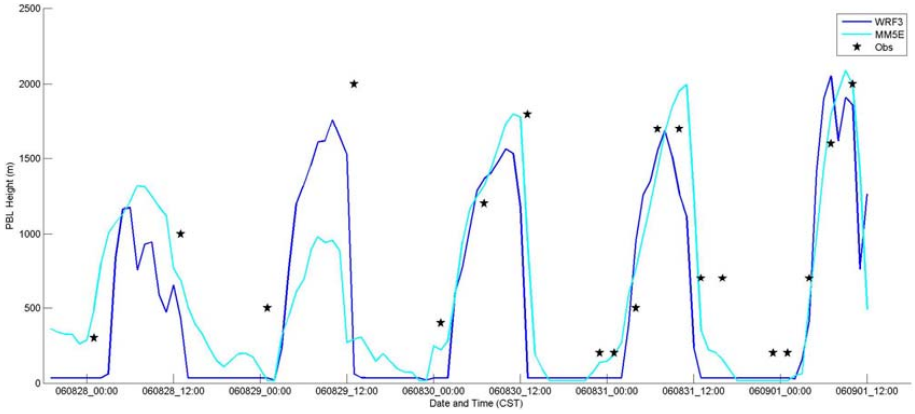

Fig. 7. Comparison of observed and simulated PBL height for the study period. The WRF simulation tended to underestimate more than either of the MM5 simulations.

GMDD
7, 2705–2743, 2014